

Geo-Congress 2026

GSP 378

Embankments, Dams, Slopes, and Soil Erosion

Selected Papers from Geo-Congress 2026
Salt Lake City, Utah | March 9–12, 2026

Edited by
Jack Montgomery, Ph.D., P.E.
Brady R. Cox, Ph.D., P.E.

ASCE
G-I ASCE GEO-INSTITUTE

GEOTECHNICAL SPECIAL PUBLICATION NO. 378

GEO-CONGRESS 2026

EMBANKMENTS, DAMS, SLOPES, AND SOIL EROSION

SELECTED PAPERS FROM SESSIONS OF GEO-CONGRESS 2026

March 9–12, 2026
Salt Lake City, Utah

SPONSORED BY

The Geo-Institute
of the American Society of Civil Engineers

EDITED BY
Jack Montgomery, Ph.D., P.E.
Brady R. Cox, Ph.D., P.E.

Published by the American Society of Civil Engineers

Published by American Society of Civil Engineers
1801 Alexander Bell Drive
Reston, Virginia, 20191-4382
www.asce.org/publications | ascelibrary.org

Any statements expressed in these materials are those of the individual authors and do not necessarily represent the views of ASCE, which takes no responsibility for any statement made herein. No reference made in this publication to any specific method, product, process, or service constitutes or implies an endorsement, recommendation, or warranty thereof by ASCE. The materials are for general information only and do not represent a standard of ASCE, nor are they intended as a reference in purchase specifications, contracts, regulations, statutes, or any other legal document. ASCE makes no representation or warranty of any kind, whether express or implied, concerning the accuracy, completeness, suitability, or utility of any information, apparatus, product, or process discussed in this publication, and assumes no liability therefor. The information contained in these materials should not be used without first securing competent advice with respect to its suitability for any general or specific application. Anyone utilizing such information assumes all liability arising from such use, including but not limited to infringement of any patent or patents.

ASCE and American Society of Civil Engineers—Registered in U.S. Patent and Trademark Office.

Photocopies and permissions. Permission to photocopy or reproduce material from ASCE publications can be requested by sending an e-mail to permissions@asce.org or by locating a title in ASCE's Civil Engineering Database (http://cedb.asce.org) or ASCE Library (http://ascelibrary.org) and using the "Permissions" link.

Errata: **Errata, if any, can be found at https://doi.org/10.1061/9780784486733**

Copyright © 2026 by the American Society of Civil Engineers.
All Rights Reserved.
ISBN 978-0-7844-8673-3 (PDF)
Manufactured in the United States of America.

Preface

This is the fourth volume of seven Geotechnical Special Publications (GSPs) containing papers from Geo-Congress 2026: Geo Tools, Technologies, and Techniques in an Environment of Change, held in Salt Lake City, Utah, on March 9-12, 2026. Notably, this conference marks the 30th anniversary of the Geo-Institute. The conference brought together industry leaders, researchers, and practitioners to showcase innovations, address critical challenges, and advance knowledge in geotechnical engineering. The conference hosted the Terzaghi, Peck, Seed, and Prakash Lectures and many technical sessions, panel sessions, short courses, and student competitions.

These proceedings represent the culmination of nearly two years of effort by the program committee and many other individuals, whose focus has been to continue the success of previous Geo-Congresses and to celebrate 30 years of geotechnical innovation by the Geo-Institute. Building the program started with an international call for papers that resulted in more than 800 abstracts on a variety of important topics. Each paper was subjected to a rigorous technical review by two or more independent peer reviewers. Acceptance required concurrence by at least two peer reviewers, and final decisions were made only after review coordinators confirmed that authors satisfactorily addressed any reviewer comments on their original submission. All accepted papers are presented at the conference as posters or technical talks and are eligible for applicable ASCE awards.

This volume contains a collection of 59 papers focused primarily on the topics of embankments, dams, slopes, landslides, and soil erosion. This includes papers on slope stability, analysis and control of erosion, modeling and assessment of landslides, and applications of remote sensing.

The success of this conference and proceedings would not have been possible without the participation and collaboration of many individuals, including Brad Keelor, the tireless staff at the Geo-Institute, and the many session chairs and reviewers. We hope that these proceedings will be of use to the geotechnical engineering community for many years to come.

The Editors,

Jack Montgomery, Ph.D., P.E., M.ASCE, Auburn University
Brady R. Cox, Ph.D., P.E., M.ASCE, Utah State University

© ASCE

Acknowledgments

We are very grateful for the contributions of the authors, peer reviewers, session chairs, and program committee, without whom this publication would not be possible.

Geo-Congress 2026 Conference Program Committee

Conference Chairs
K. N. Gunalan, Ph.D., P.E., BC.GE, Pres. 20 ASCE, NAC, HNTB Corporation
Ryan B. Maw, P.E., G.E., BC.GE, F.ASCE, Gerhart Cole

Technical Chair
Shideh Dashti, Ph.D., M.ASCE, University of Colorado Boulder

Proceedings Editors
Brady R. Cox, Ph.D., P.E., M.ASCE, Utah State University
Jack Montgomery, Ph.D., P.E., M.ASCE, Auburn University

Student Program Liaison
Cassandra Rutherford, Ph.D., P.E., M.ASCE, Iowa State University

Program Committee Members
Aaron L. Leopold, P.E., M.ASCE, Dan Brown and Associates
Kam Ng, Ph.D., P.E., M.ASCE, University of Wyoming
Jenny Ramirez, Ph.D., P.E., M.ASCE, Geosyntec Consultants

© ASCE

Contents

Embankments, Dams, and Slopes

A Framework for Landslide Susceptibility Mapping for Minnesota Using Multi-Layer Perceptron Neural Network **1**
Ambikesh Dwivedi and Surya Sarat Chandra Congress

A Physics-Informed Neural Network for Hydraulic Diffusivity Inversion in Rainfall-Induced Landslide Analysis **16**
Shian Cao and Weibing Gong

A Stress–Deformation Modeling Approach to Support Adaptive Geotechnical Design and Risk-Informed Decision Making **26**
Saeed N. Moghadam, David Walter, and Jeffrey Keaton

An ML-Based System for the Early Detection of Earth Slope Failures Using IoT Sensing Technology **35**
Mehnaz Hossain Antora, Fyaz Nafin Rahman, Rahul Debnath, Omar El Miloudi, Md. Jobair Bin Alam, and Ahmed Abdelmoamen Ahmed

Applications of Aerial LIDAR Datasets for 3D Probabilistic Slope Stability Analysis of Transportation Geotechnical Infrastructure Assets **46**
Raja Jaladurgam, Surya Sarat Chandra Congress, Raul Velasquez, Jason Hedeen, Thomas F. Wolff, and Bora Cetin

Assessing Landslide Risk and Susceptibility in Michigan's Upper Peninsula: A Case Study of the 2003 Rockland Incident **60**
Yasaman Abdolvand and Mohammadhossein Sadeghiamirshahidi

Assessing Landslide Susceptibility in a Changing Climate: Integrating Future Land Use Scenarios **70**
Nabin Budhathoki and Yuderka Trinidad González

Assessment of Analytical and Numerical Methods for Stability of Embankments over Deep Mixed Columns-Improved Soft Ground under Undrained Conditions **81**
Haohua Chen, Jie Han, and Robert L. Parsons

Assessment of Expanded Clay Aggregate for Use in Railroad Embankments **91**
Behdad Mofarraj, Saeed Goodarzi, and Jack Moore

Assessment of Satellite-Based Remote Sensing Methods for Levee Monitoring **100**
Debayan Ghosh, Puneet Bhaskar, Vinaykrishnan Lakshminarayanan, and Anand Puppala

© ASCE

Back Analysis of a Rapid Drawdown Failure at Sparmos Dam Using UAV-Based 3D Failure Geometries **110**
Jhih-Rou Huang and Dimitrios Zekkos

Considerations for Levee Design Using Staged Construction in Southeast Louisiana: A Case Study of the Design and Construction of the West Shore Lake Pontchartrain Levee **120**
James M. Williams, Sean G. Walsh, Richard J. Varuso, Jehu B. Johnson, and Leeland J. Richard

Coupled Hydro-Mechanical Analysis of Rainfall Induced Shallow Slope Instabilities **133**
Rupsa Roy, Beena Ajmera, and Binod Tiwari

Cut-Off Wall Construction of the Bastora Dam: Seepage Solution **145**
Bestun J. Shwan, Yassen W. Azeez, and Khalil K. Hamadamin

Deciphering Landslide Formation and Evolution Processes: A Time Series Interferometric Synthetic Aperture Radar-Based Investigation **155**
Xiong Bi, Yichuan Zhu, and Joseph Coe

Deep Neural Network-Based Landslide Susceptibility Mapping in Himachal Pradesh: A Comparative Study with Conventional Models **165**
Shivam, Rizul Sharma, and Kunjari Mog

Displacement Patterns of Clay Embankments Subject to Weather-Driven Deterioration under a Changing Climate **177**
Amr M. Morsy

Effects of Predicted Large Intensity Storms on Moisture Conditions and Stability of Engineered Slopes **186**
Alex B. Lefever and Kyle A. Kershaw

Establishing Cumulative Rainfall Thresholds for Landslide Early Warnings in Seattle Using Weather Data **196**
Boneng Chen and Weibing Gong

Estimating Boulder Impact Energies in Avalanches Using the Discrete Element Method **206**
Fan Yi and Fernando E. Garcia

Evaluation of Geometric Factors on Coupled Failure Mechanisms in Loaded Slopes Stabilized with Piles **215**
Irem Zeynep Yildirim and Emre Tekdemir

© ASCE

Evaluation of Slope Stability of Tailings Storage Facility under Static and Seismic Conditions **226**
Siwadol Dejphumee, James Devereaux, and Timothy Adams

Ground Movement Forensics and Sustainable Stabilization Techniques **242**
Clara Klamm, Bhaskar Chittoori, Nick Hudyma, and Seth Olsen

Harnessing Machine Learning for Railway Damage Assessment and Prediction **250**
Cyrus D. Bahman, H. Omar Ulloa, Jasmine Bekkaye, Daniel Gallegos, and Navid H. Jafari

Hybrid Approach Combining Machine Learning and Physics-Based Modelling: A Shirur Landslide Case Study Using SCOOP-3D and Random Forest **260**
Priyajit Kundu, Sreevalsa Kolathayar, and Pruthviraj Umesh

Impact of Rainfall Variability on Landslide Stability: A Study on Chattogram Hill Tracts Using GeoStudio Software **271**
Mahmudur Rahman, Md. Azijul Islam, and Md. Anisur Rahman Dip

Impact of Reservoir Fluctuations on Cracking and Erosion: Physical Modeling and Numerical Investigation **281**
Amanda Sampaio, Jaden Ladd, Jonathan Kurien, and Yuderka Trinidad González

Improving Landslide Susceptibility Mapping with Drone and Helicopter Surveys **290**
Maiely Minozzo

Influence of Terrain Model Resolution on Rockfall Dispersion **299**
Lucas Arsenith, Grant Goertzen, Nick Hudyma, and Bhaskar Chittoori

Influence of Xanthan Gum on Compaction and Shear Strength Behavior of Kaolinite and Loess **309**
Rupsa Roy, Edward Asamoah, Beena Ajmera, Cassandra Rutherford, Yuderka Trinidad González, Lucas A. Walshire, Ethan T. Vroman, Mohammed Mohammed, and Benjamin R. Breland

Investigating Hydro-Mechanical Responses of Copper Mine Tailings Dams: Insights from Numerical Simulations of Upstream, Downstream, and Centerline Designs **320**
Akshay Kumar Singh and Anumita Mishra

Laboratory Modeling of Rainfall-Induced Slope Failure in a Controlled Soil Box Setup **330**
Amin Mohammadzadeh, Mir Ali Hosseini, and Omid Ghasemi-Fare

© ASCE

Landslide Displacement Prediction Using Interferometric Synthetic Aperture Radar and Machine Learning Techniques 340
Yuxin Yuan and Lei Wang

Load Transfer Platforms for Column-Supported Embankments: A Comparative Study 347
Ashutosh Kumar Singh and Anumita Mishra

Modeling of Static Liquefaction-Induced Failure of a Tailings Storage Facility (TSF) 356
Alfonso Cerna-Diaz, Richard Davidson, Masood Kafash, Lisa Yenne, Pooya Sheykhloo, and Emad Ghodrati

Post-Wildfire Shallow Landslide Susceptibility Assessment following the January 2025 Palisades Wildfire in Southern California 373
Hao-Qing Yang, Farshid Vahedifard, and Ben A. Leshchinsky

Rockfall Hazard Assessment in Pennsylvania through Coupled Monitoring and Modeling 383
EunSik Choi, Sarah Burghardt, Jonathan Hubler, Virginia Smith, and Sarah McInnes

Sevier Bridge Dam Rehabilitation, Phase II 392
Richard Buhler, Jed McFarlane, Ryan Cole, Travis Gerber, and Phil Gerhart

Simplified Method for Consideration of Soil Arching in 2D Limit Equilibrium Slope Stability Analyses of Pile-Stabilized Embankments 407
James A. McKelvey III and Miguel A. Pando

Sodium Alginate-Based Surface Stabilization of Erosion-Prone Levee Surface: A Laboratory Rainfall Simulation Study 416
Suhyuk Park, Dongcheon Lee, Saebom Kim, and Ilhan Chang

Stability Analysis of Slow-Moving Landslides Incorporating Rate-Dependent Strength 426
Xiang Li, Alexander Handwerger, Rob Skarbek, and Giuseppe Buscarnera

Stabilizing a Landslide to Preserve the Historic Irishtown Bend in Cleveland, OH 436
T. C. Michael Law, Walter Kaeck, and Joseph Ferenczy

The Effect of Root Depth on Slope Stability with Varying Rainfall Intensities 452
Sophia K. Andanje, Pegah Ghasemi, and Brina M. Montoya

The Effects of Multiple Loading Events on Backward Erosion Piping Progression 462
Deepika Ghorasaini and John Rice

© ASCE

The Influence of Storm Time Series Characteristics on Landslide Triggering within a Watershed in Utuado, Puerto Rico 472
Mirna Kassem and Dimitrios Zekkos

The Utah Thistle Landslide of 1983: A Historical Perspective.....483
Blaine D. Leonard

UAV-Enabled Multispectral Sensing for Autonomous Surface Detection of Animal Burrows at Levees.....498
Mingliang Tang, Dimitrios Zekkos, Adda Athanasopoulos-Zekkos, and Kenichi Soga

Wellpoint Dewatering at Weston Lake Dam, Fort Jackson, South Carolina 509
Graham Elliott, Brett W. Dodd, Cole W. W. Gibson, and Richard H. Wargo

Geotechnics of Soil Erosion

Assessment of Erosive Conditions at Cumberland Island National Seashore in Southeast Georgia 521
Christopher Harrigan, Raphael Crowley, Cigdem Akan, and Christopher Bender

Impact of Atmospheric Conditions on the Erosion Potential of Burned Soil 531
Calvin Tohm and Bret Lingwall

Erodibility Assessment of Clay Modified with Lime and Recycled Materials.....541
Mahsan Keshavarz and Wilson F. Espinoza

Evaluating the Use of Fertilizer and Compost on Vegetation Growth, Sediment, and Nutrient Loss.....552
Oguzhan Saltali, Angela Farina, Mikayla Cunningham, Vincent Mwangi, Ahmet H. Aydilek, Allen P. Davis, and Bora Cetin

Experimental Study of Biopolymer Soil Stabilization of a Peruvian Coastal Sand.....563
Guillermo J. Zavala, Miguel A. Pando, Dennis Leyva, and Rafael Aguilar

Modeling Effects of Biopolymer Treatment on the Overtopping Performance of an Earthen Embankment 574
Brock M. Huner, Ethan T. Vroman, Lucas A. Walshire, Anna K. Lancaster, and Jack Montgomery

Modifying Soil Plasticity Using Biochar to Prevent Soil Erosion.....585
Fei Wang, Eunsung Kan, and Jie Huang

Particle Breakage in Hurricane Hilary-Induced Post-Wildfire Debris Flows in San Bernardino Forest 595
Lucia Landaverde Robles and Ingrid Tomac

© ASCE

Preliminary Assessment of the Interplay among the Capillary Rise, Atmospheric Evaporation, and Aeolian Sand Erosion.....605
Paula Sarmiento Robles, Luis Zambrano-Cruzatty, and Georgia Doore

Subsidence beneath Our Aging Infrastructure: A Laboratory Study on Soil Internal Erosion.....616
Giselle Morocho Aguilar, Jiahao Huang, and Wei Li

Sustainable Soil Erosion Control with Fungi.....625
Zaid Alajlan, Allen Yu, and Xiong (Bill) Yu

© ASCE

A Framework for Landslide Susceptibility Mapping for Minnesota Using Multi-Layer Perceptron Neural Network

Ambikesh Dwivedi[1] and Surya Sarat Chandra Congress[2]

[1]Graduate Student, Dept. of Civil and Environmental Engineering, Michigan State Univ. Email: dwivedi8@msu.edu
[2]Assistant Professor, Dept. of Civil and Environmental Engineering, Michigan State Univ. (corresponding author). Email: surya@msu.edu

ABSTRACT

A landslide is a geo-hazard that occurs due to the dislocation of soil or rock mass from the parent mass in the direction of gravitational force. Landslide events, often caused by a combination of natural and human-made factors, result in loss of lives and damage to property. In Minnesota, Wisconsin, and Michigan, approximately $6.7 million are spent annually on infrastructural repairs due to slope failures and landslides. Moreover, these failures cause major traffic delays, disrupt local businesses, and pose life-threatening risks to the nearby communities. Identification of landslide-susceptible zones can help improve urban management and prioritize the areas that need immediate remediation. Many factors can affect the trigger of a landslide event. The relationship between the landslide and its influencing factors is nonlinear. Artificial neural networks, mimicking the brain structure, offer a powerful tool for establishing and studying the non-linearity between variables. In the present study, a framework was demonstrated considering seven landslide influencing factors for modeling of the landslide susceptibility (LS) map for Minnesota. The LS map was developed using a multi-layer perceptron (MLP) neural network. In the current study, 7,700 landslide events in Minnesota and 7,707 non-landslide events were captured from various databases and considered for the development of the MLP model. The LS map for the study area was developed using the MLP model, which uses 70% and 30% of the dataset as the training and validation datasets, respectively. The accuracy obtained using the validation dataset was around 94.85%, indicating the “excellent”, match category. The developed LS map will be very helpful in guiding the state agencies to a better understanding of slope stability and plan for mitigation strategies.

INTRODUCTION AND BACKGROUND

Slope instability is one of the common geological hazards in hilly terrains. When the slope dimensions are significant, the resulting large failure is termed a landslide (Hungr et al., 2014). In a landslide, the soil or rock mass volume is dislocated from the parent mass toward the gravitational force to reach a state of force equilibrium. Annually, they result in severe casualties and property loss worldwide (Froud & Petley, 2018). Landslides and related slope instability phenomena can cause significant problems, including damage to infrastructure, destabilization of roads, and hazards associated with road cuts near hillsides (Singh et al., 2025). Landslides in the state of Minnesota, United States of America (USA), have caused significant damage to infrastructure and natural resources and have resulted in fatalities in the past. According to the regional data reported by Walkinshaw (1992), the total cost of contracted landslide repairs in Minnesota, Wisconsin, and Michigan in 1990 was $2.7 million annually, which is equivalent to

© ASCE

$6.7 million annually in 2025. This significant repair cost highlights the substantial public spending associated with slope failures in the Upper Midwest.

Typically, the loss due to the landslide can be classified under two categories: direct and indirect loss (Crawford, 2014). The direct loss included damage to the infrastructure and human life. Meanwhile, indirect losses are the losses that occur due to the collateral effect of the landslide mass, such as traffic disruptions due to road blockage, which can reduce the country's economic productivity (Mirus et al., 2020). Kroha and Slosson (1976) estimated that the monetary loss of $400 million caused by the 1976 landslide in Los Angeles, which is equal to $2.3 billion in 2025. The actual number can be even higher, as these damage estimations only included direct losses incurred to private dwellings.

There are several causative factors, including rainfall and earthquakes, that can trigger or exacerbate landslides (Froud & Petley, 2018; Dwivedi et al., 2024). Generally, sliding occurs along a plane when the shear stress exceeds the shear strength of the soil in the slope mass. Understanding and identifying the contributing factors or triggering mechanisms for landslides is crucial for devising effective remediation measures to stabilize the slope system. However, implementing these techniques across vast areas of natural slopes is very expensive and cumbersome. Hence, it is important to identify those critical areas where slopes are more prone to instability and prioritize the implementation of remediation techniques. Identifying and prioritizing the landslide-prone areas based on the hazard level assessment map will help the federal and state entities implement the landslide disaster mitigation policy and techniques. Moreover, it will be helpful to the departments of transportation (DOT), cities, and urban management agencies to plan the construction of infrastructure accordingly.

The frequency or probability of landslide events in an area defines its landslide susceptibility. A higher frequency means the area is more prone to landslide events (Varnes, 1984). The landslide hazard on a map can be indicated using the landslide susceptibility (LS), which shows how much an area is more prone to landslides. Various researchers have utilized GIS platforms as mapping tools to display information across multiple layers of the area (Lee & Sambath, 2006). Hence, GIS can be a powerful tool for developing an LS map of a region. Various methods are available in the literature to develop the LS map. The integration of statistical techniques with GIS methods for developing the LS map provides a reliable and effective approach for assessing landslide susceptibility (Saha & Saha, 2021). In the GIS environment, there are four available methods, namely, qualitative, semi-quantitative, quantitative, and hybrid methods, to calculate LS (Kaur et al., 2017).

The qualitative method includes two models: distributary analysis and geomorphic analysis. However, a key drawback of the qualitative method is its reliance on subjective expert judgment, which can introduce bias and reduce reproducibility (Kanungo et al., 2006). The semi-quantitative method has four models, namely, analytical hierarchy approach (AHP), fuzzy set-based analysis, weighted linear combination, and ordered weighted average. All of these come under the multi-criteria decision making (MCDM) model analysis. The disadvantage of the semi-quantitative approach is that it still uses subjective component weighting, which could compromise model prediction judgment (Pourghasem et al., 2018). Quantitative methods address this limitation of the semi-quantitative approach by using field data and statistical models instead of relying on expert judgment or scoring systems. This makes the results more objective, consistent, and accurate. Moreover, they also allow for better prediction and analysis based on field-collected data (Daniel et al., 2021). Some of the quantitative methods to develop an LS map include relative frequency ratio (RFR) (Gudiyangada Nachappa et al., 2020), artificial neural

© ASCE

networks (Pradhan & Lee, 2010), and support vector machine (Tien Bui et al., 2015). These methods use the landslide inventory data and make a relationship between the landslide causative factors and the occurrence of landslides. In the past, many researchers have used quantitative methods to map the landslide susceptibility of an area in GIS using RFR, logistic regression method, and support vector machine (SVM), assuming a linear relationship between the landslide and its influencing factors. However, in the literature, it has been established that the relationship between the landslide and its causative factors is not linear (Nefeslioglu et al., 2008; Pradhan & Lee, 2010).

An artificial neural network (ANN) is a robust machine learning algorithm used to solve and analyze the nonlinear relationship between dependent and independent variables. Hence, ANN can be a good tool in mapping landslide susceptibility if we treat landslides as dependent variables and causative factors as independent variables. Susena et al. (2025) conducted landslide susceptibility analysis for the Dieng Mountainous Region, Central Java, Indonesia, using random forest (RF), SVM, and ANN. For ANN architecture, the authors considered two hidden layers with 32 and 16 neurons in each layer, respectively, with the rectified linear unit (ReLU) as the activation function. They observed that the ANN model achieved the highest AUC value of 0.994 compared to the RF model's AUC value of 0.977, and the SVM model's AUC of 0.908.

In past years, hybrid methods have also been used in landslide susceptibility mapping because of their ability to combine the strengths of the other three methods discussed above. This method combines statistical, machine learning, and expert judgment techniques to improve the model's prediction accuracy (Kaur et al., 2017). Some of the methods under these approaches, which have been used in the past, are RFR-AHP (Fatah et al., 2024), RFR-random forest (RF) (Arabameri et al., 2019), RF-convolutional neural network (CNN) (Wang et al., 2025), etc. However, in the present study, an ANN, a quantitative method, was used to develop the landslide susceptibility model. ANN was selected in the present study to allow for a focused evaluation of the ANN's standalone performance in landslide susceptibility mapping.

Minnesota has experienced many landslides throughout its history, with records in the Twin Cities area dating back to 1879. In northwestern Minnesota near Crookston, rotational landslides have been recorded since 1933, with a major highway damaged in 2003. Notable recent events include the 2013 Lilydale Park landslide in St. Paul, where heavy rain, foot traffic, and groundwater led to the death of two children. Despite these frequent landslide events, there is no regional-scale landslide susceptibility map for the state of Minnesota. Hence, in the present study, a landslide susceptibility map of the state of Minnesota was developed, which can help the state and policymakers identify the regions that need immediate prevention. For this purpose, a framework involving ANN was demonstrated to develop the landslide susceptibility map having a resolution 3m×3m for the state of Minnesota in the U.S. Seven different causative factors, including soil, slope, curvature, elevation, aspect, land use and land cover (LULC), and twenty-year annual average rainfall, were considered as variables. Firstly, the study conducted a multicollinearity analysis to evaluate the correlation among those variables. Once the independence between variables was identified, an ANN methodology was developed to generate the LS map for Minnesota. The Minnesota map is divided and color-coded into five different landslide-susceptible zones (LSZ), namely very low, low, medium, high, and very high. Furthermore, the performance indices and a confusion matrix were provided to enhance the understanding of the ANN's performance and its potential for future research in this area. The study concluded with salient observations from the LSZ map and how federal and state agencies can use this information.

© ASCE

FRAMEWORK

In the present study, an ANN-based framework established by past studies (Pradhan & Lee, 2010; Huang et al., 2020; Liu et al., 2025; Susena et al., 2025) was used to develop the landslide susceptibility map of Minnesota, as demonstrated in the below sections.

Study Area. Minnesota is one of the Midwestern states of the United States of America. It covers a total of 225,163 square kilometers in the USA and is ranked 12th (area-based) among all the states in the USA. It spans between longitude 89°29′ W to 97°14′ W and latitude 43°30′ N to 49°23′ N. Minnesota is divided into 87 counties as of 2025 (Figure 1), in which Minneapolis, the capital of Minnesota, is in Hennepin County. According to the U.S. Census Bureau, as of July 1, 2024, the state's total population was 5.8 million, ranking it 22nd among all states in the USA. The elevation of the state ranges from 183 m to 701 m above the mean sea level. The highest elevation point of the state is at Eagle Mountain, which is in the North of Cook County and only 13 miles away from the lowest elevation point. The lowest elevation of the state is near Lake Superior. Despite some areas having steep hills or high elevations, most of the state is made up of gently rolling land that has been smoothed out over a long period of time (Ojakangas, 1982). The slope angle of the state's profile varies from 0 degrees to 88 degrees. The area receives an annual average rainfall of 452.7 mm to 812.8 mm. Due to these contributing factors, several landslide events occur in the state every year, resulting in infrastructure damage and loss of human life.

Landslide Inventory. The collection of the landslide historical data was the first step toward the development of the LS map. It is one of the crucial steps, as the accuracy of the LS map will depend on the ground truth of the landslide points. In the present study, the landslide historical data or landslide inventory was collected from different sources and grouped to form a big dataset containing 7710 landslide points, as shown in Figure 1a. The landslide dataset used in the present study was compiled by Delong et al. (2022). This inventory includes landslides detectable in 1-meter LiDAR or remote imagery at a 1:4000 scale, documented historically, or confirmed in the field. Although this approach provides a comprehensive dataset, it might have omitted small and shallow landslides, and thus cannot guarantee complete coverage. We calculated the centroids of the Landslide area polygons reported by DeLong et al. (2022) and plotted them in ArcGIS. The centroid of each landslide polygon was taken as the landslide datapoint. The sampling of non-landslide points is critical in the modelling of the susceptibility in the region. Following the approach presented by Gu et al. (2024), the present study created a 500-meter buffer zone around each landslide point to create non-landslide points. In case of overlapping buffer zones around two close landslide points, the zones were dissolved into a single unified polygon to avoid duplication and ensure distinct sampling areas. Subsequently, the same number of non-landslide points were randomly generated within the area, as shown in Figure 1b.

Factors Contributing to Landslides. There are many natural and man-made factors (e.g., rainfall, earthquake) that contribute to the triggering of the landslide. These causative factors directly or indirectly influence the landslide initiation. In the present study, seven landslide causative factors, namely, soil, twenty-year annual average rainfall, elevation, slope angle, aspect, curvature, and land use and land cover (LULC) of the study area, were considered in the analysis. The resolution of these data used for the analysis significantly impacts the accuracy obtained in the LS map. Lower-resolution data does not effectively capture the variability of the feature, as it generalizes a pixel value for an area depending on the resolution of the data.

© ASCE

Meanwhile, the higher resolution data better captures the variability of the area, shows the intricate nature of the captured surface, and provides detailed information about the area. Hence, data resolution is one of the critical aspects of analyzing a GIS environment. In the present study, all the input data were in the form of raster images having a resolution of 3m×3m, except the twenty-year annual average rainfall, with a resolution of 55km×55km, and the LULC map with a resolution of 10m×10m. Both maps were then resampled to 3m resolution. As data at 3m were not available, the lower resolution maps were resampled. This may introduce interpolation error, does not enhance the actual spatial detail, and may affect the model's precision. However, resampling was done to maintain consistency with other input layers. The data were collected from different sources, as shown in Table 1.

Table 1. Input data and its corresponding source.

Thematic Map	Source
Landslide inventory map	United States Geological Survey (USGS), Minnesota Natural Resource Atlas
Soil map	Food and Agriculture Organization of the United Nation (FAO)
Slope map, Curvature map, Elevation map, and Aspect map	Minnesota Department of Resources (MnDNR)
Land use land cover (LULC) map	Environmental System Research Institute (ESRI)
Twenty-year annual average rainfall map	University of East Anglia – Climate Research Unit (CRU)

Geological factor. The type of soil predominantly present in the study area was taken as the geological factor that can affect the landslide events. The occurrence of landslides is greatly influenced by the type of soil that forms the sloping terrain. Because of the low coefficient of permeability, fine-grained soils take longer to drain the percolated rainwater within the soil mass. As a result, there is an increase in pore water pressure, which lowers the effective normal stress and, ultimately, reduces the shear strength, which leads to slope failure. The study area's soil map was derived from the Food and Agriculture Organization of the United Nations (FAO) soil map. As illustrated in Figure 1c, the entire area was classified based on the most prevalent soil in the region.

Hydrological factors. The twenty-year annual average rainfall was taken as the hydrological factor. Most landslide incidents are caused by rainfall (Pham et al., 2017). The intensity, frequency, and duration of rainfall events significantly impact the failure mass of landslides. Rainfall causes an increase in driving forces on the sloping ground relative to opposing forces, which causes the soil mass to slide along the weaker failure plane. The CRU data site provided the rainfall data with a resolution of 55km×55km. This data was then used to create the study area's 20-year annual average rainfall map, which was then resampled into a raster map with 3m × 3m pixels, as shown in Figure 1d.

Topographical factors. Topographical characteristics that influence the landslide occurrence include the slope, aspect, curvature, and elevation of the sloping soil mass. In the present study, the MnDNR DEM data with a resolution of 3m×3m was used to create all the thematic maps of

© ASCE

topographical elements for the study area. The location's elevation has an indirect impact on the frequency of landslides (Pham et al., 2017). It controls other landslide-causing variables, such as vegetation type, rainfall, and human activity. The study area has an elevation ranging from 125m to 700 m. The elevation map of the study area in the raster format is shown in Figure 1e.

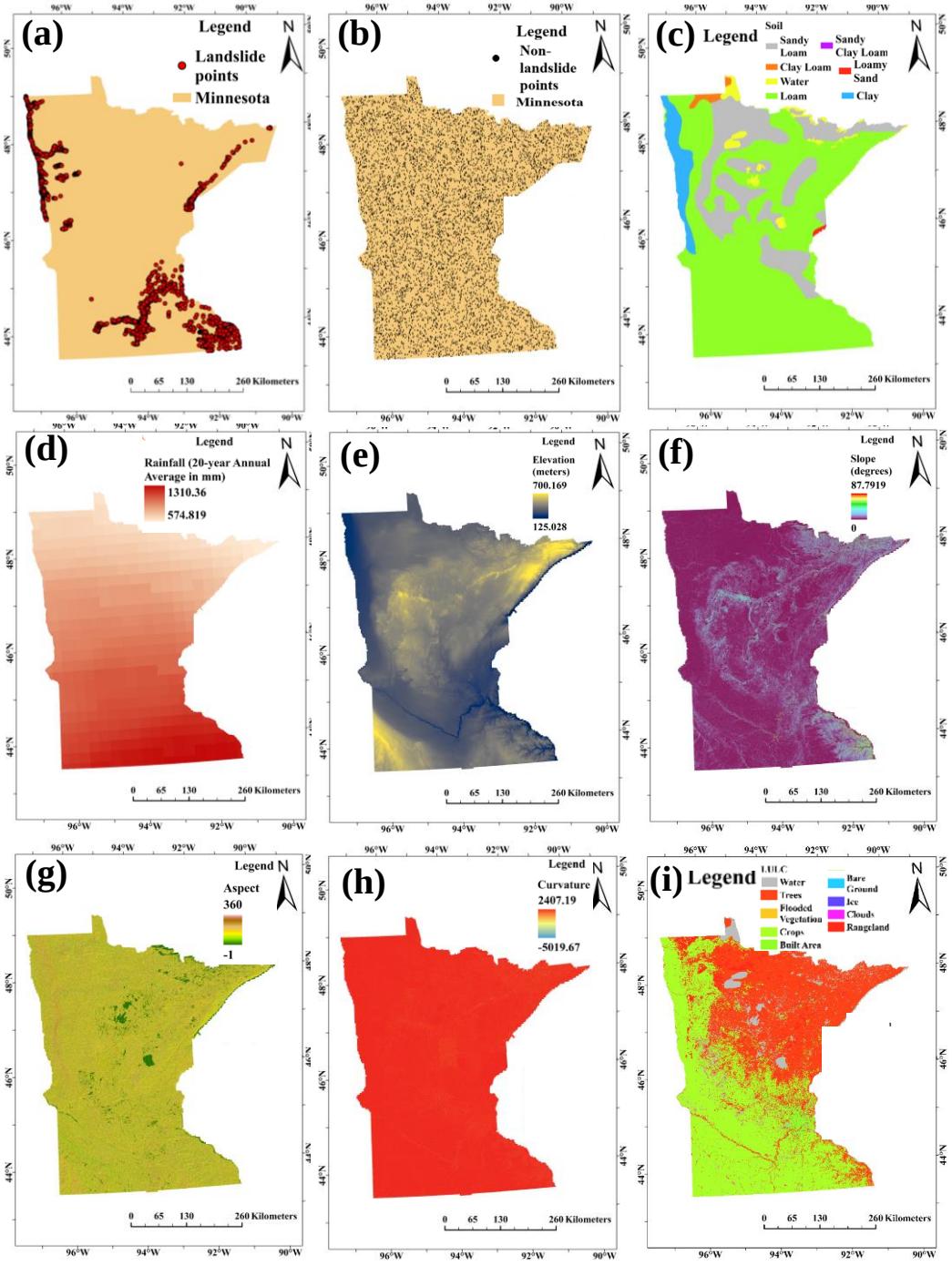


Figure 1. Study area (a) landslide points, (b) non-landslide points, (c) soil map, (d) twenty-year annual average rainfall map, (e) elevation map, (f) slope map, (g) aspect map, (h) curvature map, (i) LULC map.

© ASCE

Slope angle is defined as the angle between the horizontal plane and the surface of the terrain. It is a measure of the steepness, typically expressed in degrees or percent. The likelihood of landslides is significantly influenced by the slope's angle at which the soil mass rests. The amount of soil weight that contributes to the sliding increases with an increase in the slope angle. Moreover, because of the high water velocity on steep slopes during rainfall, surface soil erodes, and percolated water adds to the soil system's driving force, making slopes more susceptible to instability. The present study area has a slope ranging from 0 to 88 degrees. The slope map of the study area in the raster format is shown in Figure 1f.

The aspect of the slope determines how much sunshine or wind it is going to receive (Ercanoglu & Gokceoglu, 2004), which controls the moisture and temperature of the location and indirectly controls the microbiology of the location. It indirectly influences many sub-parameters, which contribute to a landslide. The aspect map of the study area was classified into ten classes, namely, north, northeast, east, southeast, south, southwest, west, northwest, north, and flat, as shown in Figure 1g. The areas having a zero-degree slope angle were considered flat.

The slope's curvature significantly Influences the flow characteristics of the water or debris mass across the slope. It dictates whether the flowing mass will accelerate or decelerate, which means it influences whether the surface will erode or receive deposition from the flowing material. The flowing mass at the crown will slow down if the slope has an upward convex surface. In contrast, the flowing mass will accelerate at the slope's crown when the surface is concave, and soil mass from the crown area will erode. The curvature map for the study area in the raster format is shown in Figure 1h. The negative value classes show areas with convex surfaces upward, and the positive value classes show areas with concave surfaces upward.

Anthropogenic factors. The LULC was taken into account in order to evaluate the impact of anthropogenic influences on landslides. The LULC map helps identify the area's habitat characteristics and classifies them as water, crops, forests, etc. The slope's habitat feature significantly influences the occurrence of landslides. A dense forest on the slope, for instance, will lessen the likelihood of landslides, but a bare location will increase the likelihood of landslides. The LULC map of the study area was taken from ESRI with 10m×10m resolution (10m×10m is the highest resolution data available presently) and then resampled into the required 3m×3m raster format, as shown in Figure 1i.

Multicollinearity Analysis. Seven factors, namely soil, slope, curvature, elevation, aspect, land use and land cover (LULC), and twenty-year annual average rainfall, were considered as the causative factors for the landslide. These factors were selected based on their well-established influence on slope stability, as supported by previous landslide susceptibility studies (Ecranoglu et al., 2004; Kanungo et al., 2008; Pham et al., 2017; Daniel et al., 2021). They represent key geological, hydrological, topographical and anthropogenic factors that contribute to landslide occurrences. For the ANN modelling, these variables need to be independent for generating an accurate landslide susceptibility (LS) map (Yi et al., 2022). Firstly, a multicollinearity analysis needs to be done to analyze the correlation between the landslide causative factors. In the present study, an index called the variance inflation factor (VIF) was calculated to analyze the multicollinearity of the different variables considered in the study. To calculate the VIF for a given variable (X_i), the correlation of determination (R_i^2) is calculated between the first variable under focus and the rest of the variables. Once R_i^2 is calculated, the VIF for each variable X_i can be calculated using Eq. 1. A variable can be called an independent variable among the given set of variables if the VIF calculated is lower than 10 (Dou et al., 2020). Moreover, an additional index called tolerance (TOL) was calculated, which is the Inverse of VIF (Eq. 1). If the value of

© ASCE

TOL is greater than 0.1, it indicates the independence of variables among the given set of variables (Wang et al., 2020).

$$VIF = \frac{1}{1-R_i^2} = \frac{1}{TOL} \quad (1)$$

Once it was established that the landslide causative factors considered were independent variables (i.e., the VIF value should be lower than 10 and the TOL value should be higher than 0.1), the landslide susceptibility (LS) modeling can be done using ANN.

Artificial Neural Network Modeling. Artificial Neural Network (ANN) is a powerful machine-learning (ML) technique that is primarily used to analyze the dependent and independent variables for complex nonlinear behaviour of a problem. ANN models have several advantages over traditional methods, such as high accuracy, capturing non-linearity, handling of high-dimensional data, and strong robustness (Pradhan & Lee, 2010). The structure of the ANN mimics the operation and structure of the human nervous system. Generally, the structure of the ANN consists of an input layer, hidden layers, and an output layer, as shown in Figure 2. Each layer consists of neurons interconnected with the next layer's neurons by weights. The number of hidden layers used in a particular problem is dependent on the complexity of the problem. A trial-and-error approach is required to identify the optimal number of hidden layers to analyze a given problem. The neurons of the hidden and output layers contain the activation functions that formulate the complex relationship between the dependent and independent variables to make predictions.

Ground truth data refers to the actual observed values, which serve as a reference for comparing predictions and evaluating the performance of the ANN model. In the present study, ground truth refers to the actual classification of landslide locations, where 0 denotes non-landslide areas and 1 denotes landslide occurrences. During the model training, these weights are updated with the back-propagation algorithm (Liu et al., 2025), which penalizes the weights by calculating the error between the ground truth and the predictions. There are many types of ANNs, such as multi-layer perceptron (MLP), recurrent neural network (RNN) (Isazade et al., 2025), convolutional neural network (CNN) (Hakim et al., 2022), autoencoders (Huang et al., 2020), and generative adversarial networks (GANs) (Jiang et al., 2025). Broadly, these ANNs are classified into feed-forward and recurrent neural networks. In the feed-forward neural networks, the information flows only in one direction without any recurrent loop of information. Feed-forward neural networks are simple and easy to train. However, they are not suitable for temporal analysis as they cannot retain past information or handle sequential data effectively. Recurrent neural networks (RNNs) are suitable for sequential data, such as time series and language data analysis. Moreover, RNNs are capable of learning temporal pattern analysis, which is essential in considering the temporal variation (e.g., rainfall) affecting landslides (Isazade et al., 2025). However, these types of ANNs are more complex, slower to train, and prone to vanishing gradient problems. In the present study, MLP was used to model the LS map of the state of Minnesota. MLP is a type of feed-forward neural network that consists of at least one hidden layer between the input and output layers.

In the present study, a total of 7710 landslide points within the study area were collected from various sources listed in Table 1. Subsequently, the same number of non-landslide points were randomly generated within the area. After that, the landslide points were labeled as 1, and non-landslide points were labeled as 0, which simplified the LS mapping task into a binary classification problem. Once the landslide and non-landslide location points were labeled, the

© ASCE

pixel values from the causative factor raster map corresponding to these points were extracted. After that, the whole dataset was randomly split into a 70:30 ratio. 70% of the dataset was used for training, whereas the remaining 30% of the dataset was used for validating the trained model.

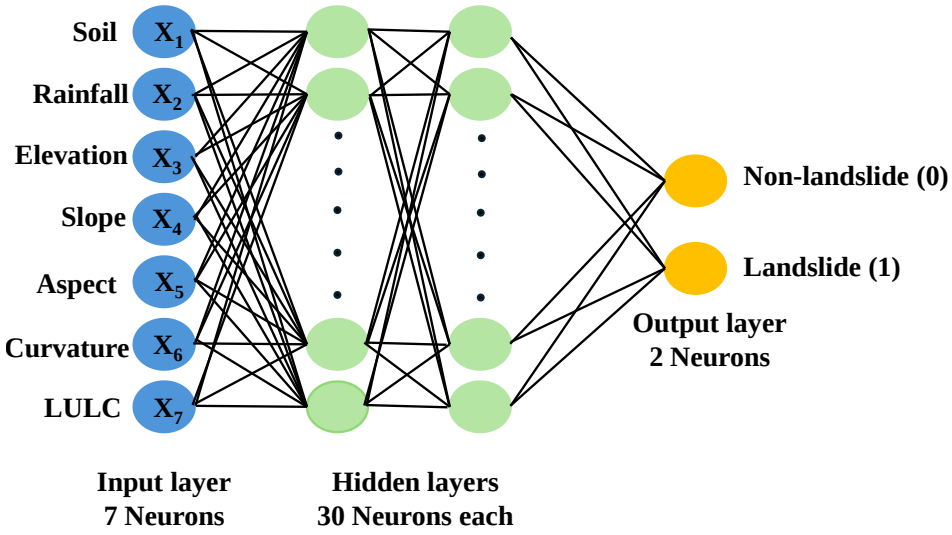


Figure 2. Multi-layer perceptron (MLP) structure in the present study.

The MLP used for the current study consists of one input layer, two hidden layers, and one output layer. The input layer consists of seven neurons, where each neuron represents a landslide causative factor. The output layer consists of two neurons for landslide and non-landslide outputs, respectively. Rectified linear unit (ReLU) and sigmoid functions were used as the activation functions in the hidden layers and output layer, respectively. Meanwhile, a trial-and-error approach was adopted to obtain the number of hidden layers and the optimal number of neurons in the hidden layers for the desired accuracy of the model. A trial-and-error approach is necessary because there is no fixed rule for determining the number of hidden layers and the optimal number of neurons in hidden layers; it helps identify the architecture that provides the best model accuracy and generalization. In trial and error analysis, the number of hidden layers varied from 1 to 3, and the number of neurons in the hidden layers was varied from 10 to 50. After trial and error, it was identified that two hidden layers and thirty neurons in each of the hidden layers yielded the highest testing accuracy. After training the MLP model with the training dataset, the validation dataset was used to evaluate the performance of the trained model. Furthermore, the performance metrics such as accuracy, precision, recall, and F1 score were calculated on the validation dataset by using Eqs. 2, 3, 4, and 5, respectively. Moreover, the confusion matrix was produced to gain insight into the model's performance. A confusion matrix consists of four parameters, namely true positive, true negative, false positive, and false negative. True positive (TP) is a landslide sample that is correctly predicted as a landslide by the model, and true negative (TN) is a non-landslide sample that is correctly predicted as a non-landslide by the model. Meanwhile, false positive (FP) is a non-landslide sample that is incorrectly predicted as a landslide by the model, and false negative is a landslide sample that is incorrectly predicted as non-landslide by the model.

© ASCE

$$Accuracy = \frac{TP+TN}{TP+TN+FP+FN} \quad (2)$$

$$Precision = \frac{TP}{TP+FP} \quad (3)$$

$$Recall = \frac{TP}{TP+FN} \quad (4)$$

$$F1\ score = 2 \times \frac{Precision \times Recall}{Precision+Recall} \quad (5)$$

where TP is true positive, TN is true negative, FP is false positive, and FN is false negative.

MODELING AND RESULTS

The results of the multicollinearity analysis are shown in Figure 3. From the analysis, it was found that the values of VIF and TOL for all the causative factors were within the threshold limit, i.e., the VIF values were lower than 10 and TOL values were higher than 0.1. This implies that the landslide causative factors were independent (Dou et al., 2020; Yi et al., 2022), and there is no significant collinearity among them. Hence, the ANN modeling was performed considering the seven causative factors as independent variables.

For the ANN model training, the optimal number of iterations was 40, as it was observed that the model loss decrement was very little after 40 iterations. Hence, 40 iterations were optimal for training the present MLP model. After fixing the optimal iterations, trial and error was done to obtain the optimal number of neurons in the hidden layers. The neurons were varied from 10 to 50 in the hidden layers, and the model was trained. After the trial and error analysis, it was found that the model validation accuracy increased up to 30 neurons in the hidden layers, and after that, the increment in accuracy was almost negligible. Hence, the MLP model with 30 neurons in the hidden layers was considered ideal for the present study.

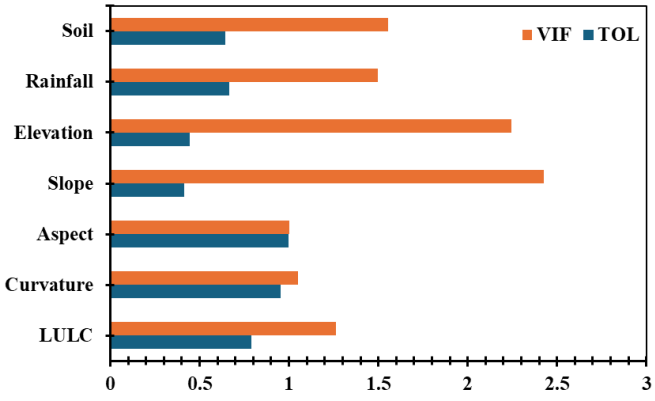


Figure 3. Multicollinearity analysis result.

The LS map obtained from the MLP modeling had values ranging from 0 to 1, where 0 shows the region non-susceptible to landslides, and the higher values closer to 1 show the area more prone to landslides. Following the methodology proposed by Yingze et al. (2024**)**, the

© ASCE

whole study area is divided into five different landslide-susceptible zones (LSZ), namely very low, low, medium, high, and very high, depending on the LS map pixel values, as shown in Figure 4a. The areal distribution of the LSZ map is shown in Figure 4b. It can be seen from Figure 4b that a total of 7.14% and 33.20% of the whole state of Minnesota were found to fall under very high and high landslide susceptibility zones, respectively. However, a thorough field investigation and verification are further needed to validate these findings of the present study.

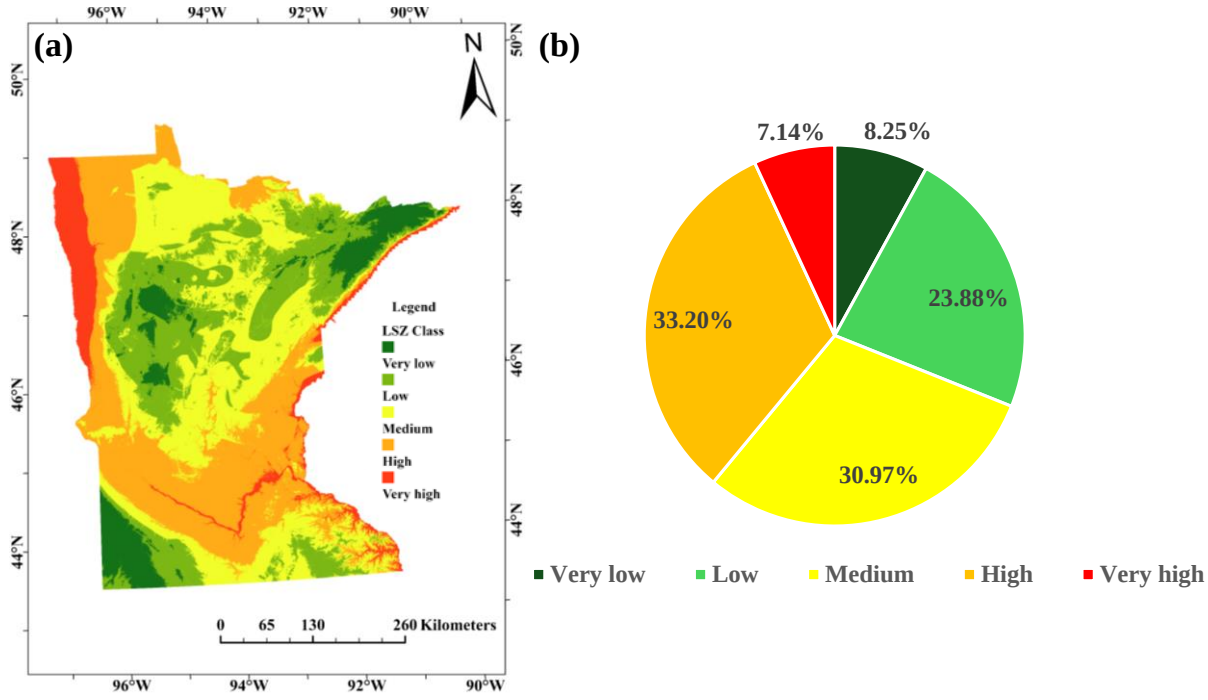


Figure 4. Landslide susceptibility analysis result (a) LSZ map, and (b) areal distribution of LSZ classes.

Validation of Landslide Susceptibility Zonation Map. In the present study, the validation of the developed MLP model was done with the help of validation data. Firstly, the validation accuracy was calculated, which was 94.85%, which shows the model's excellent performance in the landslide susceptibility classification. Further, the confusion matrix was also calculated, as shown in Figure 5. Moreover, model evaluation metrics such as precision, recall, and F1 score were calculated to validate the model's robustness and reliability, as shown in Table 2. As shown in Figure 5, the model effectively classified the landslide and non-landslide zones. In comparison, the model accuracy was better for classifying landslide zones than non-landslide zones, as the false positives were slightly higher than false negatives. Overall, the MLP model's performance in the present study area was excellent, as the values of precision, recall, and F1 score were close to 0.95 for the model. Also, the macro and weighted averages for all the metrics were equal to 0.95, showing the model's excellent performance. Macro average is the average of a metric (e.g., precision, recall, or F1-score) calculated separately for each class, giving equal weight to all classes. Meanwhile, weighted average is the average of the metrics for each class, but weighted by the number of true instances in each class.

© ASCE

Table 2. Evaluation report for the MLP model in the present study.

Description	Precision	Recall	F1-score	Accuracy
Non-landslide (0)	0.97	0.93	0.95	0.95
Landslide (1)	0.93	0.97	0.95	
Macro average	0.95	0.95	0.95	
Weighted average	0.95	0.95	0.95	

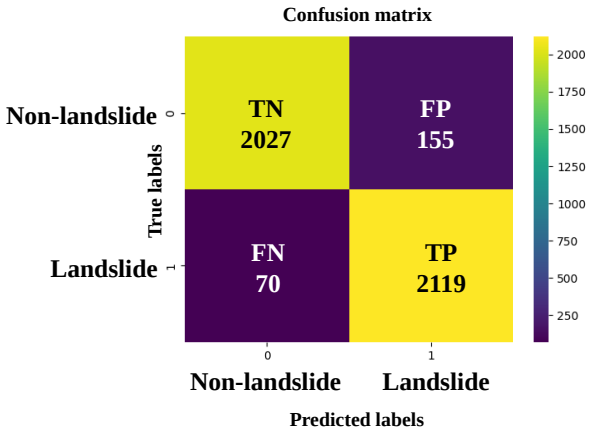


Figure 5. MLP validation result using the confusion matrix.

CONCLUSIONS

In the present study, the landslide susceptibility (LS) map of Minnesota was developed. The model was developed using a multi-layer perceptron (MLP) type neural network. Seven landslide causative factors were considered for the analysis. The MLP model was developed based on landslide inventory data. The following were the conclusions drawn from the whole study:

i. The VIF and TOL values of the causative factors were within the acceptable limit as suggested by past studies. Hence, all seven causative factors considered in the analysis were independent.
ii. The validation accuracy of the model was 94.85%, showing an excellent performance in classifying landslide and non-landslide zones.
iii. Thorough field investigations are further needed to validate the findings of the present study.
iv. After validation, the potential landslide susceptibility zonation map developed in this study helps the federal, state, and local agencies understand the conditions and prepare mitigation plans.

In the present study, a basic MLP model was used to develop the LS map of Minnesota, achieving good landslide prediction accuracy. However, existing literature shows many advanced ANN architectures that could produce even better accuracy. Moreover, as we know, the ANN is a black box model; hence, getting insight into how the causative factors are affecting the model is unknown in the present study, which is the key limitation of the present study. In future study, explainable artificial intelligence models can be utilized to better understand the relative importance and impact of each individual factor on landslide occurrence. Such insight

© ASCE

would be valuable for local and federal authorities to select the influencing parameters which are critical in developing the remedial measures and accordingly.

REFERENCES

Arabameri, A., Pradhan, B., Rezaei, K., and Lee, C. W. (2019). Assessment of landslide susceptibility using statistical-and artificial intelligence-based FR–RF integrated model and multiresolution DEMs. *Remote Sensing*, 11(9), 999.

Crawford, P. S. (2014). *Methodology for a GIS-based damage assessment for researchers following large scale disasters*. The University of Alabama.

Daniel, M. T., Ng, T. F., Abdul Kadir, M. F., and Pereira, J. J. (2021). Landslide susceptibility modeling using a hybrid bivariate statistical and expert consultation approach in Canada Hill, Sarawak, Malaysia. *Frontiers in Earth Science*, 9, 616225.

DeLong, S. B., Jennings, C. E., and Gran, K. B. (2022). Landslides in Minnesota (No. 2022-3007). US Geological Survey.

Dou, J., Yunus, A. P., Bui, D. T., Merghadi, A., Sahana, M., Zhu, Z., and Pham, B. T. (2020). Improved landslide assessment using support vector machine with bagging, boosting, and stacking ensemble machine learning framework in a mountainous watershed, Japan. *Landslides*, 17, 641-658.

Dwivedi, A., Jha, A. K., Hegde, A., and Singh, T. N. (2024, December). Enhancing Stability in Hilly Road Slopes: Seismic Stability Analysis and Material Optimization for a Two-Lane Expansion in Meghalaya, India. In *International Conference on Recent Advances in Geotechnical Earthquake Engineering and Soil Dynamics* (pp. 119-129). Singapore: Springer Nature Singapore.

Ercanoglu, M. U. R. A. T., Gokceoglu, C. A. N. D. A. N., and Van Asch, T. W. (2004). Landslide susceptibility zoning north of Yenice (NW Turkey) by multivariate statistical techniques. *Natural Hazards*, 32, 1-23.

Fatah, K. K., Mustafa, Y. T., and Hassan, I. O. (2024). Geoinformatics-based frequency ratio, analytic hierarchy process and hybrid models for landslide susceptibility zonation in Kurdistan Region, Northern Iraq. *Environment, Development and Sustainability*, 26(3), 6977-7014.

Froude, M. J., and Petley, D. N. (2018). Global fatal landslide occurrence from 2004 to 2016. *Natural Hazards and Earth System Sciences*, 18(8), 2161-2181.

Gu, T., Duan, P., Wang, M., Li, J., and Zhang, Y. (2024). Effects of non-landslide sampling strategies on machine learning models in landslide susceptibility mapping. *Scientific reports*, 14(1), 7201.

Gudiyangada Nachappa, T., Kienberger, S., Meena, S. R., Hölbling, D., and Blaschke, T. (2020). Comparison and validation of per-pixel and object-based approaches for landslide susceptibility mapping. *Geomatics, Natural Hazards and Risk*, 11(1), 572-600.

Hakim, W. L., Rezaie, F., Nur, A. S., Panahi, M., Khosravi, K., Lee, C. W., and Lee, S. (2022). Convolutional neural network (CNN) with metaheuristic optimization algorithms for landslide susceptibility mapping in Icheon, South Korea. *Journal of environmental management*, 305, 114367.

Huang, F., Zhang, J., Zhou, C., Wang, Y., Huang, J., and Zhu, L. (2020). A deep learning algorithm using a fully connected sparse autoencoder neural network for landslide susceptibility prediction. *Landslides*, 17, 217-229.

© ASCE

Hungr, O., Leroueil, S., and Picarelli, L. (2014). The Varnes classification of landslide types, an update. *Landslides*, 11(2), 167-194.

Isazade, V., Qasimi, A. B., Namivandi, M. S., Amin, M. S., and Ahlem, G. (2025). Landslide Susceptibility Assessment Using Recurrent Neural Network (RNN)—A Case of Chabahar and Konarak in Iran. *Indian Geotechnical Journal*, 1-21.

Jiang, Y., Wang, W., Zou, L., Cao, Y., and Xie, W. C. (2025). Investigating landslide data balancing for susceptibility mapping using generative and machine learning models. *Landslides*, 22(1), 189-204.

Kanungo, D. P., Arora, M. K., Gupta, R. P., and Sarkar, S. (2008). Landslide risk assessment using concepts of danger pixels and fuzzy set theory in Darjeeling Himalayas. *Landslides*, 5, 407-416.

Kaur, H., Gupta, S., and Parkash, S. (2017). Comparative evaluation of various approaches for landslide hazard zoning: a critical review in Indian perspectives. *Spatial Information Research*, 25, 389-398.

Krohn, J. P., and JE, S. (1976). Landslide Potential In the United States.

Lee, S., and Sambath, T. (2006). Landslide susceptibility mapping in the Damrei Romel area, Cambodia using frequency ratio and logistic regression models. *Environmental Geology*, 50, 847-855.

Liu, S., Jiang, X., He, X., Qiu, H., Yang, Y., Zhao, R., and Hu, H. (2025). A novel landslide susceptibility mapping method based on a backpropagation neural network algorithm with optimized non-landslide samples and hyperparameters. *Engineering Applications of Artificial Intelligence*, 155, 111052.

Mirus, B. B., Jones, E. S., Baum, R. L., Godt, J. W., Slaughter, S., Crawford, M. M., and McCoy, K. M. (2020). Landslides across the USA: occurrence, susceptibility, and data limitations. *Landslides*, 17, 2271-2285.

Nefeslioglu, H. A., Duman, T. Y., and Durmaz, S. (2008). Landslide susceptibility mapping for a part of tectonic Kelkit Valley (Eastern Black Sea region of Turkey). *Geomorphology*, 94(3-4), 401-418.

Pham, B. T., Tien Bui, D., and Prakash, I. (2017). Landslide susceptibility assessment using bagging ensemble based alternating decision trees, logistic regression and J48 decision trees methods: a comparative study. *Geotechnical and Geological Engineering*, 35, 2597-2611.

Pradhan, B., and Lee, S. (2010). Delineation of landslide hazard areas on Penang Island, Malaysia, by using frequency ratio, logistic regression, and artificial neural network models. *Environmental Earth Sciences*, 60, 1037-1054.

Pourghasemi, H. R., Teimoori Yansari, Z., Panagos, P., and Pradhan, B. (2018). Analysis and evaluation of landslide susceptibility: a review on articles published during 2005–2016 (periods of 2005–2012 and 2013–2016). *Arabian Journal of Geosciences*, 11, 1-12.

Saha, A., and Saha, S. (2021). Application of statistical probabilistic methods in landslide susceptibility assessment in Kurseong and its surrounding area of Darjeeling Himalayan, India: RS-GIS approach. *Environment, Development and Sustainability*, 23(3), 4453-4483.

Singh, H., Dwivedi, A., Jha, A. K., Hegde, A., Tripathi, A., and Singh, T. N. (2024, January). Stability Analysis of Grouted Backfill Retaining Wall for Highway Construction. In *International Conference on Geotechnical Issues in Energy, Infrastructure and Disaster Management* (pp. 615-623). Singapore: Springer Nature Singapore.

© ASCE

Susena, Y., Hadmoko, D. S., and Wibowo, S. B. (2025). Machine learning techniques on spatio-temporal data for landslide susceptibility assessment at Dieng Mountainous Region, Banjarnegara district, Central Java, Indonesia. *Natural Hazards*, 1-38.

Tien Bui, D., Shahabi, H., Shirzadi, A., Chapi, K., Alizadeh, M., Chen, W., and Tian, Y. (2018). Landslide detection and susceptibility mapping by airsar data using support vector machine and index of entropy models in cameron highlands, malaysia. *Remote Sensing*, 10(10), 1527.

Varnes, D. J. (1984). *Landslide hazard zonation: a review of principles and practice (No. 3)*.

Wang, S., Zhang, K., van Beek, L. P., Tian, X., and Bogaard, T. A. (2020). Physically-based landslide prediction over a large region: Scaling low-resolution hydrological model results for high-resolution slope stability assessment. *Environmental Modelling & Software*, 124, 104607.

Wang, Y., Wu, X., Zhou, K., Lin, G., Peng, B., and Fang, Z. (2025). Integrating a multi-dimensional deep convolutional neural network with optimized sample selection for landslide susceptibility assessment. *Geo-spatial Information Science*, 1-21.

Walkinshaw, J. (1992). *Landslide correction costs on U.S. state highway systems*. Transportation Research Record, 36-36.

Yi, X., Feng, W., Bai, H., Shen, H., and Li, H. (2021). Catastrophic landslide triggered by persistent rainfall in Sichuan, China: August 21, 2020, Zhonghaicun landslide. *Landslides*, 18, 2907-2921.

Yingze, S., Yingxu, S., Xin, Z., Jie, Z., and Degang, Y. (2024). Comparative analysis of the TabNet algorithm and traditional machine learning algorithms for landslide susceptibility assessment in the Wanzhou Region of China. *Natural Hazards*, 120(8), 7627-7652.

© ASCE

A Physics-Informed Neural Network for Hydraulic Diffusivity Inversion in Rainfall-Induced Landslide Analysis

Shian Cao, S.M.ASCE[1]; and Weibing Gong, Ph.D., M.ASCE[2]

[1]Ph.D. Student, Dept. of Civil Engineering, Univ. of Kentucky, Lexington, KY.
Email: shiancao399@uky.edu
[2]Assistant Professor, Dept. of Civil Engineering, Univ. of Kentucky, Lexington, KY.
Email: wbgong@geosensinglab.com

ABSTRACT

Rainfall-induced landslides pose a significant threat to infrastructure and communities worldwide. Their occurrence is strongly linked to the hydrodynamic behavior of slopes during intense precipitation events. Understanding the complex interactions between rainfall infiltration, pore water pressure buildup, and slope stability is critical for forecasting and mitigating these hazards. A key parameter in rainfall-induced landslide analysis is hydraulic diffusivity, which governs the rate of water movement within slopes and directly influences slope stability. However, determining hydraulic diffusivity is usually challenging because of its small magnitude, which typically ranges from the order of 10^{-8} to 10^{-3} m^2/s. Conducting field tests or collecting soil samples from potential landslide sites for laboratory tests is time-consuming, costly, and potentially hazardous due to the challenging or unsafe accessibility of such areas. Nevertheless, the estimation of hydraulic diffusivity is essential for understanding slope hydrodynamics, predicting pore pressure buildup, and assessing the timing and severity of rainfall-induced landslides. This study presents a physics-informed neural network (PINN) inversion method to estimate hydraulic diffusivity by solving the Richards equation using pressure head data that are available from field monitoring. The proposed method focuses on treating hydraulic diffusivity as a training parameter within an inverse problem, leveraging one of the key advantages of PINNs in inversion analysis. The inverted parameter can then be utilized to assess hydrological responses induced by future rainfall events. The results of a case study show that this method can achieve an accuracy of 98.8% in estimating hydraulic diffusivity using only 30 sets of observation data with 6 designed sensors. These results highlight the proposed method's potential to rapidly inform slope stability assessments, improve landslide forecasting, and enhance disaster preparedness in landslide-prone regions.

INTRODUCTION

In recent decades, the increasing frequency of extreme weather events has exacerbated the incidence of landslides (Emberson et al. 2021; Miller et al. 2021), one of the most prevalent natural hazards in mountainous areas (Froude and Petley 2018; Abdollahi et al. 2024). Unexpected rainfall, a common trigger for these events, poses significant risks to both infrastructure integrity and human life (Guzzetti et al. 2008; Froude and Petley 2018; Lü et al. 2024). For instance, an extreme rainfall event in 2023 delivering 320 mm of precipitation within 48 hours affected Fuyang in Zhejiang Province, China, inducing over 145 landslides and causing five fatalities (Lü et al. 2024).

© ASCE

To quantify the impacts of rainfall on slopes, Iverson (2000) proposed a rainfall-induced landslide assessment model to evaluate the transient pore pressure response to rainfall, and compute key stability parameters including factor of safety (FS), failure timing, and landslide velocity. Moreover, the Iverson model has been developed to address more complex conditions (e.g., Tsai and Yang 2006; Tsai et al. 2008) and incorporated into practical computational tools such as the TRIGRS model developed by the USGS (Baum et al. 2002; Baum et al. 2010), owing to its minimal parameter requirements and high feasibility.

Despite its feasibility, the Iverson model critically depends on the estimation of hydraulic diffusivity, which is incorporated within the governing partial differential equation (PDE). It exerts significant control over landslide stability by modulating the transient response of pore pressure to infiltration (Han et al. 2020; Das et al. 2022). Accordingly, the determination of hydraulic diffusivity is critical for accurate landslide forecasting. However, measuring hydraulic diffusivity is challenging in both laboratory and field settings due to its extremely low magnitude (usually below 10^{-3} m²/s) (Bear 1972) and strict testing procedures (Coutinho et al. 2019). Moreover, conducting such tests in landslide-prone areas poses significant risks.

Recent advances in physics-informed neural networks (PINNs), which efficiently solve PDEs by combining physical laws with data-driven models, provide a feasible method to address the above challenges (Raissi et al. 2019; Karniadakis et al. 2021; Lu et al. 2021). PINNs offer greater feasibility under limited data for solving inverse problems than conventional methods by considering unknown parameters as extra training inputs, making them particularly suitable for estimating hydraulic diffusivity in the Iverson model.

This study introduces a PINN approach to estimate hydraulic diffusivity from monitored slope pressure head data. This method utilizes one of the core advantages of PINNs in inversion analysis, treating the hydraulic diffusivity as a trainable parameter, along with slope depth and time as inputs. The estimated hydraulic diffusivity can then be incorporated into future landslide forecasting analyses. The feasibility of this method is demonstrated through a previously reported case study. Compared to conventional methods, this approach can yield hydraulic diffusivity estimates within minutes, providing a powerful tool for rapid rainfall-induced landslide assessment.

IVERSON MODEL FOR PRESSURE HEAD

Rainfall infiltration raises pore pressure and reduces the shear strength of the slope soil, resulting in the potential slope failure (Guzzetti et al. 2008; Froude and Petley 2018). Understanding the spatial and temporal variations of pore pressure within a slope is fundamental for evaluating landslide triggering and evolution, as these variations directly affect the FS and determine the onset, timing, and magnitude of slope failure (Iverson 2000). Accurately characterizing the pressure head distribution is therefore essential for modeling the dynamic processes underlying landslide initiation and progression. In a Cartesian coordinate system, the impact of rainfall on the near-surface pressure head is modeled by the Richards equation (Richards 1931; Bear 1972; Hurley and Pantelis 1985), which was subsequently simplified by Iverson (2000) as follows:

$$\frac{\partial \psi}{\partial t} = D_0 \cos^2 \alpha \frac{\partial^2 \psi}{\partial Z^2} \quad (1)$$

© ASCE

where ψ represents the pressure head; Z denotes the vertical depth from the slope surface; t denotes the time since rainfall; α denotes the slope angle; and D_0 represents the hydraulic diffusivity.

The initial condition (IC), and boundary conditions (BCs) of this PDE are defined as:

$$\psi(Z,0) = (Z - d_z)\beta \tag{2}$$

$$\frac{\partial \psi}{\partial Z}(\infty, t) = \beta \tag{3}$$

$$\frac{\partial \psi}{\partial Z}(0,t) = -\frac{I_Z}{K_Z} + \beta, t \le T \tag{4}$$

where T denotes the rainfall duration; d_z represents the steady water table depth; I_z and K_z denote the rainfall intensity and hydraulic conductivity in the vertical direction, respectively; (I_Z/K_Z) represents the normalized infiltration rate; and β represents a constant, defined as $\beta = \cos^2\alpha - (I_Z/K_Z)_{\text{steady}}$, with $(I_Z/K_Z)_{\text{steady}}$ as the steady-state vertical water influx.

The solution of the PDE is provided by Iverson (2000) as:

$$\psi(Z, t \le T) = (Z - d)\beta + \frac{I_Z}{K_z}\left[\left(\frac{\widehat{D}t}{\pi}\right)^{\frac{1}{2}} \exp\left(-\frac{Z^2}{\widehat{D}t}\right) - Z \cdot \text{erfc}\left(\frac{Z^2}{\widehat{D}t}\right)^{\frac{1}{2}}\right] \tag{5}$$

where $\widehat{D} = 4D_0\cos^2\alpha$ represents the effective hydraulic diffusivity; and erfc represents the complementary error function.

The FS of a slope under rainfall impacts can be determined based on the pressure head as (Iverson 2000):

$$\text{FS}(Z,t) = \text{FS}_0(Z) + \text{FS}'(Z,t) \tag{6}$$

$$\text{FS}_0(Z) = F_f + F_c - \frac{\psi_0(Z)\gamma_w \tan\varphi}{\gamma_s Z \sin\alpha \cos\alpha} \tag{7}$$

$$\text{FS}'(Z,t) = -\frac{[\psi(Z,t) - \psi_0(Z)]\gamma_w \tan\varphi}{\gamma_s Z \sin\alpha \cos\alpha} \tag{8}$$

where $\psi_0(Z)$ is the initial pressure head given by Eq. (2); φ denotes the soil friction angle; c denotes the soil cohesion; F_c and F_f are the components, depending on the soil and slope physical properties; and γ_s and γ_w denote the unit weights of soil and water, respectively.

PINN-BASED INVERSION ANALYSIS

Inverse PINN modeling is employed to estimate unknown parameters from the observed data (Lu et al. 2021). In the context of landslide assessment, this study focuses on estimating hydraulic diffusivity D_0 using monitored pressure head data ψ. Conventional hydraulic field testing typically utilizes water level indicators and pressure transducers to record underground pressure head. However, determining hydraulic diffusivity prior to every rainfall event is unrealistic for practical engineering applications. This challenge arises from several factors: (i)

© ASCE

Hydraulic diffusivity is highly site-specific, varying with soil type, porosity, saturation levels, and antecedent moisture conditions (Bear 1972), which precludes the establishment of universal reference values without direct measurement; (ii) Standard in-situ testing methods (e.g., piezometer-based monitoring, pumping tests, and borehole infiltration tests) require on-site instrumentation and stable field conditions that may be absent in remote or unstable terrains (Bear 1972); and (iii) Laboratory-based measurements, such as permeability tests and soil column experiments, are time-consuming and unsuitable for near real-time hazard assessments. Moreover, performing in-situ tests during active rainfall poses operational risks due to potential slope instability.

Fig. 1 presents the proposed PINN inversion analysis approach based on the Iverson model, which overcomes these limitations via a two-stage workflow. The first stage involves hydraulic diffusivity D_0 estimation, where monitored pressure head data from embedded sensors are used to inversely determine hydraulic diffusivity. In practical monitoring, it is feasible to continuously measure pressure head through hydrologic sensors such as water level indicators and pressure transducers. This approach eliminates the need for extensive soil sampling and on-site testing, thereby reducing costs and safety constraints. In the second stage, the estimated hydraulic diffusivity is integrated into a forward modeling process to evaluate slope stability under current or forecasted rainfall conditions. This integration facilitates near real-time forecasting of landslide risk and supports timely warning and mitigation efforts.

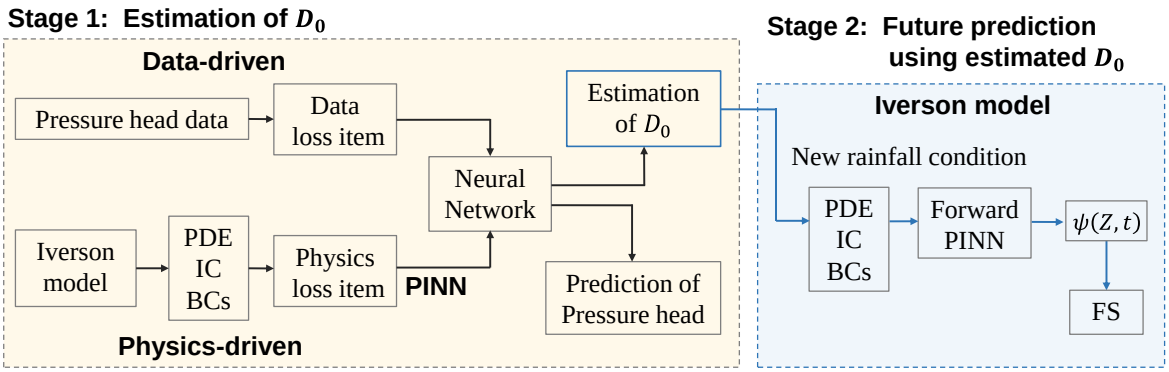


Fig. 1. Inversion analysis workflow of proposed PINN for estimating hydraulic diffusivity and assessing future potential landslides.

PINNs are a class of deep learning models designed to approximate solutions to PDEs by learning a mapping from the spatio-temporal domain to the corresponding physical response. Fig. 2 shows the PINN architecture tailored to solve the Iverson model, consisting of three key components: a neural network, a loss function, and an optimizer (Raissi et al. 2019; Karniadakis et al. 2021; Lu et al. 2021). A defining feature of PINNs is the integration of governing physical laws into the loss function as soft constraints (Lu et al. 2021). Within this framework, automatic differentiation (AD) is employed to compute the required derivatives of the network output with respect to the inputs, enabling efficient evaluation of PDE residuals. The optimizer then iteratively minimizes the loss function by updating the network parameters. Compared to conventional neural network methods, inverse PINN modeling is particularly advantageous as unknown physical parameters can be included as extra trainable variables. These parameters are optimized simultaneously with the network weights in the iteration process, guided by their

© ASCE

contribution to the total loss function. This study implements the PINN framework using the DeepXDE library (Lu et al. 2021), built on TensorFlow.

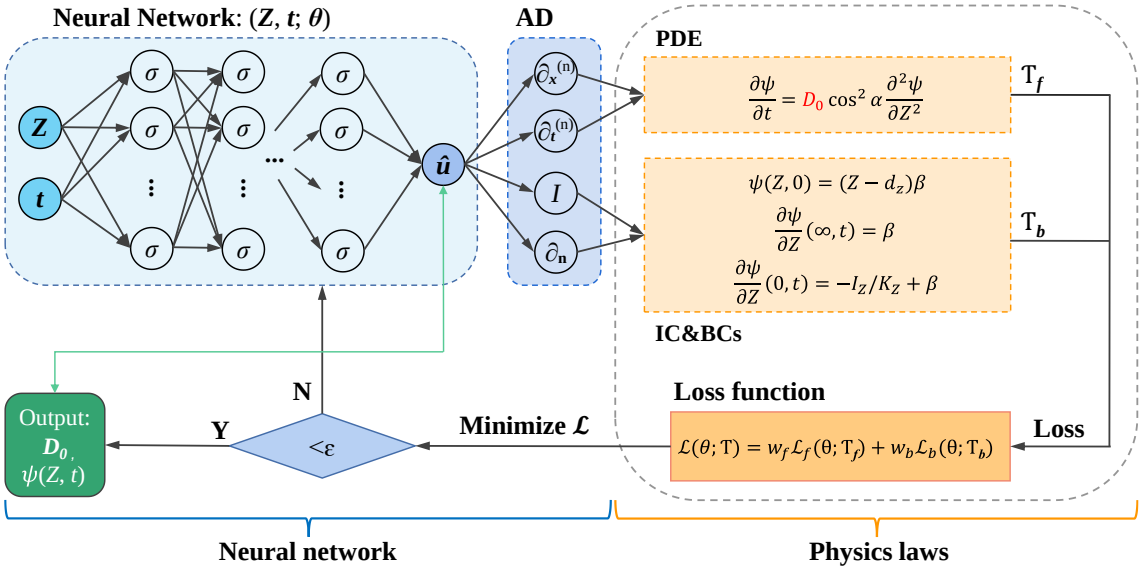


Fig. 2. PINN architecture for estimating hydraulic diffusivity and predicting pressure head.

CASE VALIDATION

Iverson (1984) reported the slow-moving and clay-rich Minor Creek Landslide, caused by prolonged rainfall in northern California. The landslide occurred at a depth of 6 m below the surface, with a slope angle (α) of 15° and a stable water table located 2 m below the surface (d_z). The soil hydraulic diffusivity (D_0) is 10^{-6} m²/s. The landslide material is characterized by a friction angle (φ) of 18° and a cohesion (c) of 4 kPa, while the saturated soil and water have unit weights (γ_s and γ_w) of 22 kN/m³ and 9.8 kN/m³, respectively. Additionally, the normalized infiltration rate (I_z/K_z) is set at 1, with a steady influx $(I_z/K_z)_{\text{steady}}$ of 0.1. The rainfall event persisted for a duration (T) of 12 weeks.

The sampling strategy employed in PINN inversion analysis generally involves uniform sampling across the entire spatiotemporal domain. However, in this study, a sampling strategy, where monitoring points are fixed at designated depths and multiple measurements are recorded, is adopted to better reflect realistic engineering conditions, thereby yielding a sparse data set. Specifically, a total of 6 monitoring points were uniformly distributed from the depth of 1 to 6 m, and 5 recordings were conducted, generating 30 distinct data points. The dataset was generated by Iverson's solution as expressed in Eq. 5. Therefore, the observation data for training in this study are synthetic and are not practically measured, but they can still demonstrate the feasibility of this framework.

To estimate hydraulic diffusivity, an inversion PINN method was implemented on an NVIDIA-T4 GPU using Google Colab. The architecture comprised a feedforward neural network (FNN) with 3 hidden layers, each containing 40 neurons. The hyperbolic tangent (tanh) activation function was employed and the Glorot uniform initializer for weight initialization was utilized. Optimization was performed using the Adam algorithm. The mean squared error was used for the residual calculation, with the weights of all loss terms set to 1. In addition, the

© ASCE

learning rate (Lr) decay was conducted in training, reducing the Lr from 10^{-3} to 10^{-4} after 40,000 iterations, to achieve better and faster results (You et al. 2019). The entire training process, including the estimation of hydraulic diffusivity and the corresponding pressure head predictions, costs 476.5 seconds (i.e., 7.9 minutes).

Figs. 3 and 4 illustrate the evolution of the loss history and the estimated hydraulic diffusivity in the training process, respectively. The PINN inversion model effectively identifies the approximate range of the unknown hydraulic diffusivity within 20,000 iterations and subsequently converges continuously toward the reference value. Correspondingly, the loss curve rapidly declines to the order of 10^{-4} within 20,000 iterations. The final estimated hydraulic diffusivity is D_0 = 9.88×10^{-7} m^2/s with a relative percentage error of 1.2%, which is in close agreement with the reference value D_0 = 10×10^{-7} m^2/s reported by Iverson (1984). The accuracy of 98.8% using only 6 sensors, confirms the accuracy and effectiveness of the proposed PINN inversion method in parameter estimation for rainfall-induced landslides.

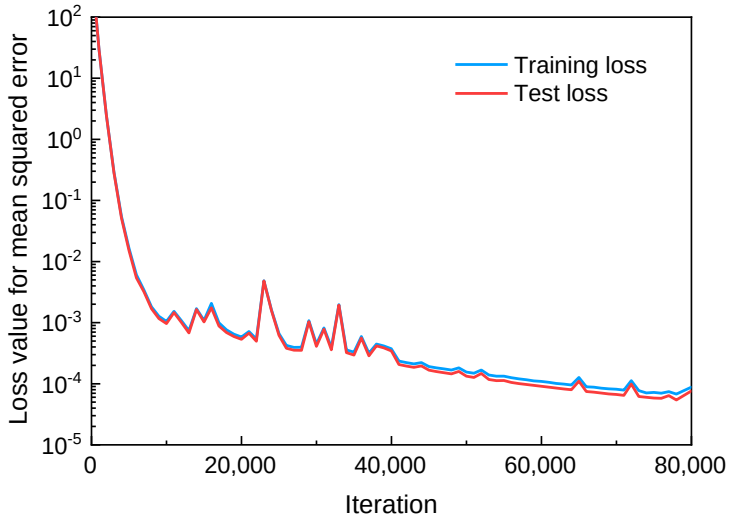


Fig. 3. Training loss history of the PINN inversion model.

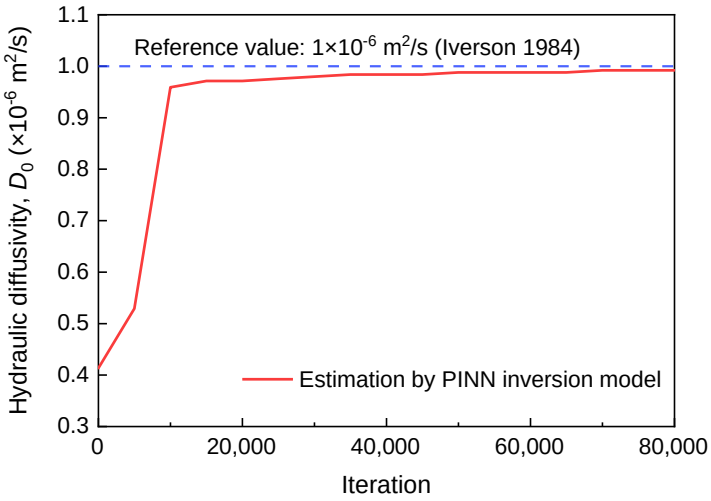


Fig. 4. Estimated hydraulic diffusivity during the training process.

© ASCE

During the training phase of the PINN inversion model, in addition to yielding the estimation of hydraulic diffusivity, the model simultaneously generates predictions for the pressure head (see Fig. 2). Fig. 5 shows the pressure head predictions derived from the PINN model. The predicted pressure head closely adheres to the theoretical calculation overall, with only a minor deviation near $(z, t) = (0,0)$ with the maximum of 0.2 m, while these errors are acceptable as we more concern about the deeper depth rather than slope surface in landslide assessment. This outcome further corroborates the robustness and efficacy of the proposed PINN inversion method in addressing the complexities associated with rainfall-induced landslides.

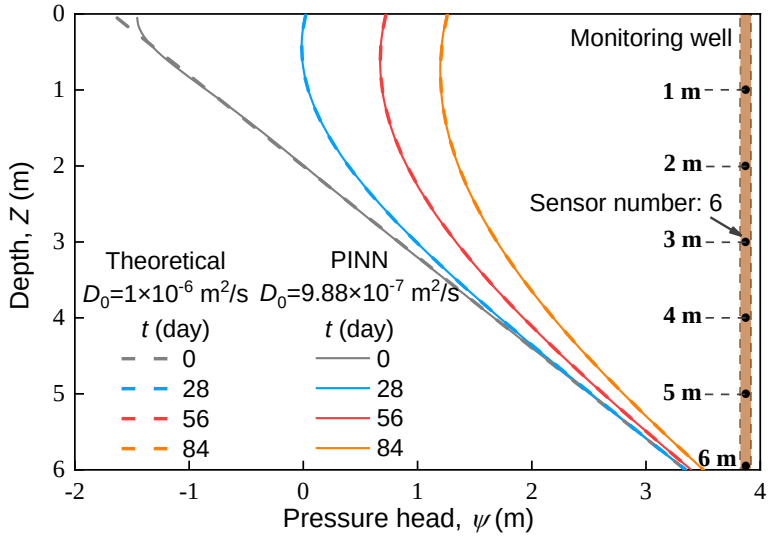


Fig. 5. Pressure head predicted by PINN inversion model.

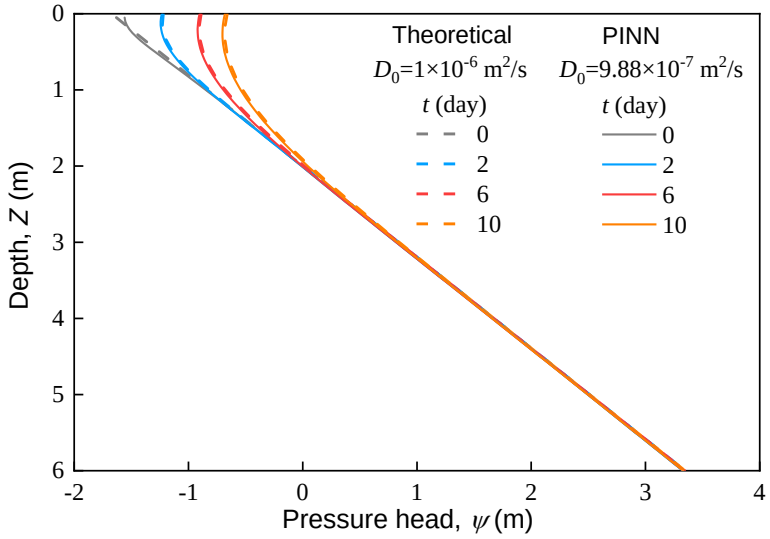


Fig. 6. Predictions of pressure head using estimated D_0 under a 10-day rainfall duration.

Fig. 6 shows the application of the previously estimated hydraulic diffusivity to pressure head predictions under another rainfall duration. The Minor Creek landslide also experienced

© ASCE

seasonal short-term rainfall (Iverson 1984), where a new rainfall duration was 10 days, while all other parameters remained the same. Through employing the hydraulic diffusivity estimated by the proposed PINN method, the PINN predictions show strong agreement with those predicted by the theoretical model. It can be observed that the overall trends of the predicted pressure head curves are generally consistent with theoretical solutions.

The complete PINN inversion analysis method comprises three sequential steps: (Step 1) the estimation of hydraulic diffusivity from observational data; (Step 2) the prediction of pressure head evolution; and (Step 3) the evaluation of FS. Fig. 7 illustrates the FS of the slope based on the pressure head predictions. It is found that the FS decreases with increasing depth. As the rainfall continues, the FS decreases slightly. However, the FS is always larger than 1 (i.e., FS $>$ 1) during the entire rainfall, which means that the slope is stable.

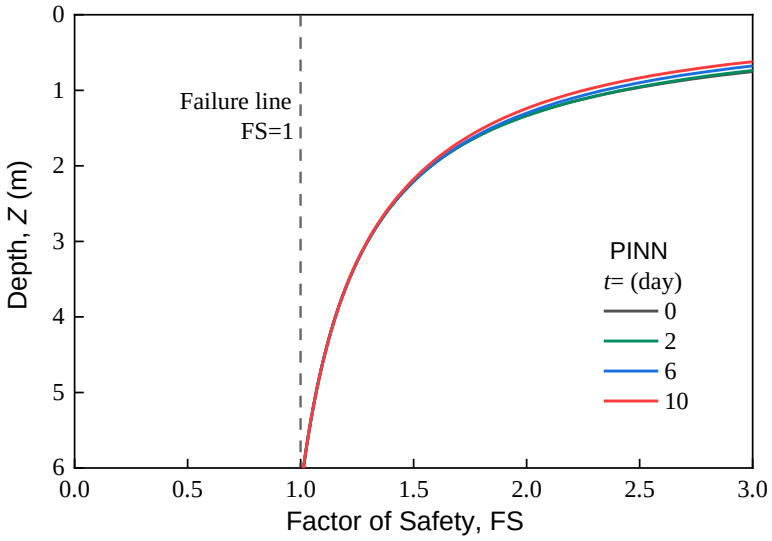


Fig. 7. Predictions of FS using estimated D_0 and pressure head under a 10-day rainfall duration.

CONCLUSIONS

This study introduces a PINN inversion method to estimate hydraulic diffusivity from slope pressure head monitoring data. By considering hydraulic diffusivity as an optimizable parameter alongside slope depth and rainfall time inputs, the proposed method leverages the intrinsic advantages of PINNs in inverse analysis. The case study demonstrated that, even with only 30 sets of monitoring data and 6 monitoring points, the proposed method can estimate hydraulic diffusivity with an accuracy of 98.8%. Unlike laboratory testing, this PINN approach can yield hydraulic diffusivity estimates within minutes using limited sensor data, thus enabling rapid and adaptive landslide risk assessment. Moreover, the estimated hydraulic diffusivity can be employed for subsequent rainfall-induced pressure head and FS predictions. This finding provides a valuable reference for achieving efficient and low-cost hydrologic parameter evaluation, which is challenging to accomplish using conventional methods in landslide-prone regions.

© ASCE

ACKNOWLEDGMENTS

This work was supported by startup funding provided to Gong by the University of Kentucky through the National Science Foundation (NSF) EPSCoR project (Cooperative Agreement No. 2344533). Any opinions, findings, conclusions, or recommendations expressed in this paper are those of the authors and do not necessarily reflect the views of NSF.

REFERENCES

Abdollahi, M., Vahedifard, F., and Leshchinsky, B. A. 2024. "Hydromechanical modeling of evolving post-wildfire regional-scale landslide susceptibility." *Eng. Geol.*, 335: 107538.

Baum, R. L., Godt, J. W., and Savage, W. Z. 2010. "Estimating the timing and location of shallow rainfall-induced landslides using a model for transient, unsaturated infiltration." *J. Geophys. Res. Earth Surf.*, 115(F3).

Baum, R. L., Savage, W. Z., and Godt, J. W. 2002. "TRIGRS—A Fortran program for transient rainfall infiltration and grid-based regional slope-stability analysis." U.S. Geol. Surv. Open-File Rep. 2002-424, U.S. Geological Survey, Reston, VA.

Bear, J. 1972. *Dynamics of fluids in porous media*. New York: Dover Publications.

Coutinho, R. Q., Silva, M. M., Santos, A. N. D., and Lacerda, W. A. 2019. "Geotechnical characterization and failure mechanism of landslide in granite residual soil." *J. Geotech. Geoenviron. Eng.*, 145(8): 05019004.

Das, P., Patwa, D., and Bharat, T. V. 2022. "Influencing factors on the simulation of rainfall-induced landslide prediction based on case study." *Bull. Eng. Geol. Environ.*, 81(5): 194.

Emberson, R., Kirschbaum, D., and Stanley, T. 2021. "Global connections between El Niño and landslide impacts." *Nat. Commun.*, 12(1): 2262.

Froude, M. J., and Petley, D. N. 2018. "Global fatal landslide occurrence from 2004 to 2016." *Nat. Hazards Earth Syst. Sci.*, 18(8): 2161–2181.

Guzzetti, F., Peruccacci, S., Rossi, M., and Stark, C. P. 2008. "The rainfall intensity–duration control of shallow landslides and debris flows: An update." *Landslides*, 5(1): 3–17.

Han, T., Liu, L., and Li, G. 2020. "The influence of horizontal variability of hydraulic conductivity on slope stability under heavy rainfall." *Water*, 12(9): 2567.

Hurley, D. G., and Pantelis, G. 1985. "Unsaturated and saturated flow through a thin porous layer on a hillslope." *Water Resour. Res.*, 21(6): 821–824.

Iverson, R. M. 1984. "Unsteady, nonuniform landslide motion: Theory and measurement." Ph.D. dissertation, Stanford Univ., Stanford, CA.

Iverson, R. M. 2000. "Landslide triggering by rain infiltration." *Water Resour. Res.*, 36(7): 1897–1910.

Karniadakis, G. E., Kevrekidis, I. G., Lu, L., Perdikaris, P., Wang, S., and Yang, L. 2021. "Physics-informed machine learning." *Nat. Rev. Phys.*, 3(6): 422–440.

Lu, L., Meng, X., Mao, Z., and Karniadakis, G. E. 2021. "DeepXDE: A deep learning library for solving differential equations." *SIAM Rev.*, 63(1): 208–228.

Lü, Q., Wu, J., Liu, Z., Liao, Z., and Deng, Z. 2024. "The Fuyang shallow landslides triggered by an extreme rainstorm on 22 July 2023 in Zhejiang, China." *Landslides*, 21(11): 2725–2740.

© ASCE

Miller, D., Forsythe, J., Kusselson, S., Straka, W., Yin, J. III, Zhan, X., and Ferraro, R. 2021. "A study of two impactful heavy rainfall events in the Southern Appalachian Mountains during early 2020, part I; societal impacts, synoptic overview, and historical context." *Remote Sens.*, 13(13): 2452.

Raissi, M., Perdikaris, P., and Karniadakis, G. E. 2019. "Physics-informed neural networks: A deep learning framework for solving forward and inverse problems involving nonlinear partial differential equations." *J. Comput. Phys.*, 378: 686–707.

Richards, L. A. 1931. "Capillary conduction of liquids through porous mediums." *Physics*, 1(5): 318–333.

Tsai, T. L., Chen, H. E., and Yang, J. C. 2008. "Numerical modeling of rainstorm-induced shallow landslides in saturated and unsaturated soils." *Environ. Geol.*, 55(3): 1269–1277.

Tsai, T. L., and Yang, J. C. 2006. "Modeling of rainfall-triggered shallow landslide." *Environ. Geol.*, 50(4): 525–534.

You, K., Long, M., Wang, J., and Jordan, M. I. 2019. "How does learning rate decay help modern neural networks?" arXiv Prepr., arXiv:1908.01878.

© ASCE